Supporting Information

Insight into the role of tunable nitrogen vacancies in transition metal nitrides for ammonia synthesis

Shiqi Yu[a], Ziyu Mei[b], Luyuan Wang[b], Yuping Ren[b], Wei Wu[a], Mao Liu*[a], Tianyi Wang*[b], Chuangwei Liu*[b,c]

[a]School of Metallurgy, Northeastern University, Shenyang 110819, China

[b]School of Material Science and Engineering, Northeastern University, Shenyang 110819, China

[c]Dalian Institute of Chemical Physics, Chinese Academy of Sciences, Dalian, 116023 China

*Corresponding Author: liumao@mail.neu.edu.cn; tianyiwang@mail.neu.edu.cn; cwliu@dicp.ac.cn

Table S1. Calculated E_{ads}, E_{vac}, N-N bond length, Bader charge of the catalytic site (i.e., δ of the metal atom), d-band center and the ΔG_{max} of NRR.

Surfaces	E_{ads} (eV)	E_{vac} (eV)	N-N (Å)	δ(e)	d-band center (eV)	ΔG_{max}^{NRR} (Distal) (eV)	ΔG_{max}^{NRR} (Alter) (eV)
CeN(100)	0.55	--	1.17	--	--	--	--
CeN(110)	0.08	--	1.14	-1.56	-1.84	1.27	1.27
CeN(111)	-0.43	--	1.17	--	--	--	--
Co_3Mo_3N(100)	-0.23	--	1.14	-0.79	-1.18	1.29	1.29
Co_3Mo_3N(110)	0.73	--	1.12	--	--	--	--
Co_3Mo_3N(211)	0.72	--	1.16	--	--	--	--
CrN(100)	0.93	--	1.12	--	--	--	--
CrN(100)-V(N)	0.73	-0.01	1.12	--	--	--	--
CrN(100)-V(N_2)	-0.66	1.61	1.14	-1.01	-1.28	2.33	2.33
CrN(110)	0.68	--	1.13	--	--	--	--
CrN(110)-V(N)	-0.02	-0.42	1.14	-1.29	0.18	0.99	0.99
CrN(110)-V(N_2)	-0.14	-0.02	1.14	-1.29	-0.73	1.79	1.79
CrN(111)	0.51	--	1.15	--	--	--	--
Fe_3Mo_3N(100)	0.39	--	1.12	--	--	--	--
Fe_3Mo_3N(110)	-0.07	--	1.12	--	--	--	--
Fe_3Mo_3N(211)	0.73	--	1.15	--	--	--	--
La_3AlN(100)	-0.91	--	1.38	--	--	--	--
La_3AlN(110)	-0.22	--	1.14	--	--	--	--
La_3AlN(111)	0.69	--	1.13	--	--	--	--
LaN(100)	-0.05	--	1.13	--	--	--	--

Surfaces	E_{ads} (eV)	E_{vac} (eV)	N-N (Å)	δ(e)	d-band center (eV)	ΔG_{max}^{NRR} (Distal) (eV)	ΔG_{max}^{NRR} (Alter) (eV)
LaN(100)-V(N)	0.73	0.50	1.13	--	--	--	--
LaN(110)	-1.49	--	1.13	--	--	--	--
LaN(110)-V(N)	-1.20	0.14	1.17	-1.50	-0.76	1.04	1.04
LaN(111)	-1.16	--	1.16	--	--	--	--
Mn_4N(100)	-0.61	--	1.12	--	--	--	--
Mn_4N(100)-V(N)	-0.22	-0.74	1.28	-0.39	-0.50	2.69	3.20
Mn_4N(100)-V(N_2)	5.61	-3.27	1.17	--	--	--	--
Mn_4N(110)	-4.07	--	1.16	--	--	--	--
Mn_4N(110)-V(N)	-1.50	-2.73	1.15	-0.40	-1.90	3.67	3.67
Mn_4N(111)	-1.76	--	1.17	-0.29	-1.52	3.60	3.60
MoN(001)	2.24	--	1.15	--	--	--	--
MoN(100)	0.97	--	1.21	--	--	--	--
MoN(111)	0.42	--	1.13	-0.29	-0.80	1.54	1.54
NbN(100)	-0.88	--	1.14	-1.72	-0.71	0.85	0.85
NbN(100)-V(N)	1.39	-1.89	1.24	--	--	--	--
NbN(100)-V(N_2)	0.11	1.12	1.22	-1.53	-0.12	1.02	1.05
NbN(100)-V(N_3)	0.51	0.39	1.21	-1.25	-0.03	1.43	1.43
NbN(100)-V(N_4)	-1.08	1.65	1.29	-1.23	-0.70	0.95	1.03
NbN(110)	-1.92	--	1.20	-1.63	-0.26	1.38	1.38
NbN(110)-V(N)	-0.52	0.35	1.20	-1.47	-0.41	1.14	1.14
NbN(111)	0.74	--	1.12	--	--	--	--

Surfaces	E_{ads} (eV)	E_{vac} (eV)	N-N (Å)	δ(e)	d-band center (eV)	ΔG_{max}^{NRR} (Distal) (eV)	ΔG_{max}^{NRR} (Alter) (eV)
ScN(100)	0.19	--	1.12	--	--	--	--
ScN(110)	0.64	--	1.12	--	--	--	--
ScN(111)	0.74	--	1.12	--	--	--	--
TiN(100)	0.73	--	1.12	--	--	--	--
TiN(110)	-0.63	--	1.19	-1.66	-0.04	1.19	1.19
TiN(111)	1.87	--	1.28	--	--	--	--
TiN(111)-V(N)	0.61	-0.70	1.12	--	--	--	--
TiN(111)-V(N_2)	0.57	1.61	1.13	--	--	--	--
TiN(111)-V(N_3)	-0.46	1.25	1.20	-1.84	0.21	1.51	1.51
TiN(111)-V(N_4)	0.22	1.45	1.22	-1.83	-0.66	1.13	1.13
YN(100)	0.30	--	1.12	--	--	--	--
YN(110)	0.52	--	1.13	--	--	--	--
YN(111)	-1.98	--	1.15	--	--	--	--

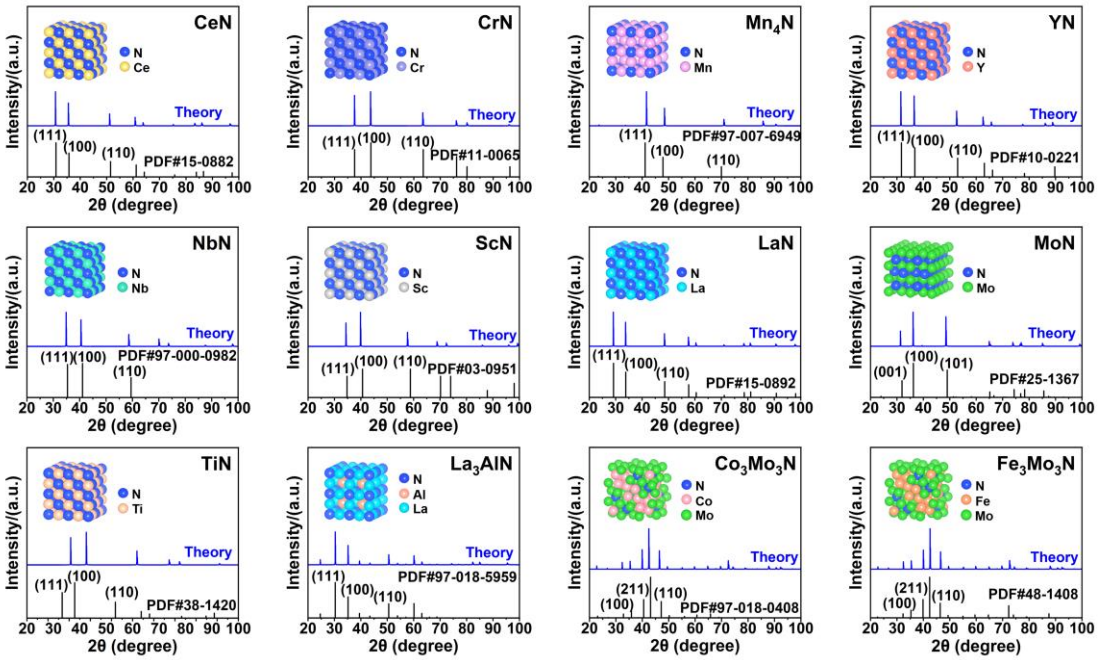

Fig. S1 Theoretically derived X-ray diffraction patterns of 12 metal nitride catalysts.

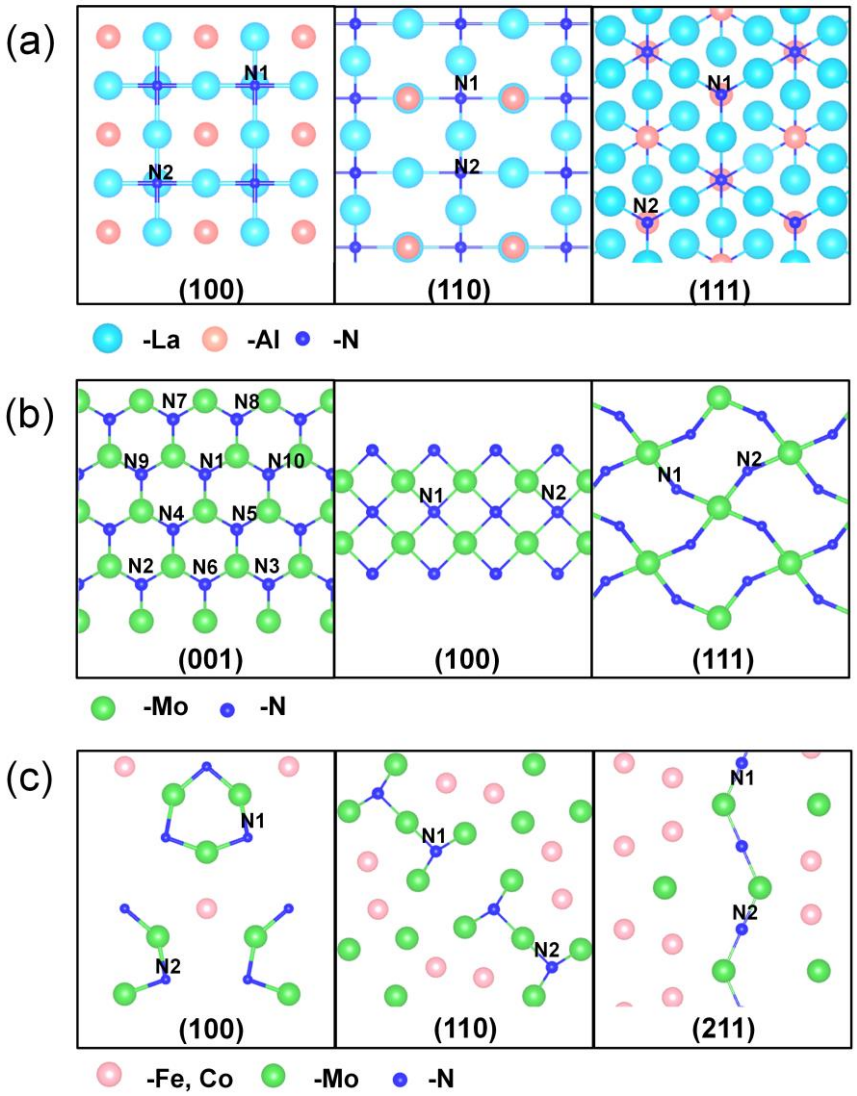

Fig. S2 Top view of the original surface of the optimized metal nitride and the location of the nitrogen vacancies.

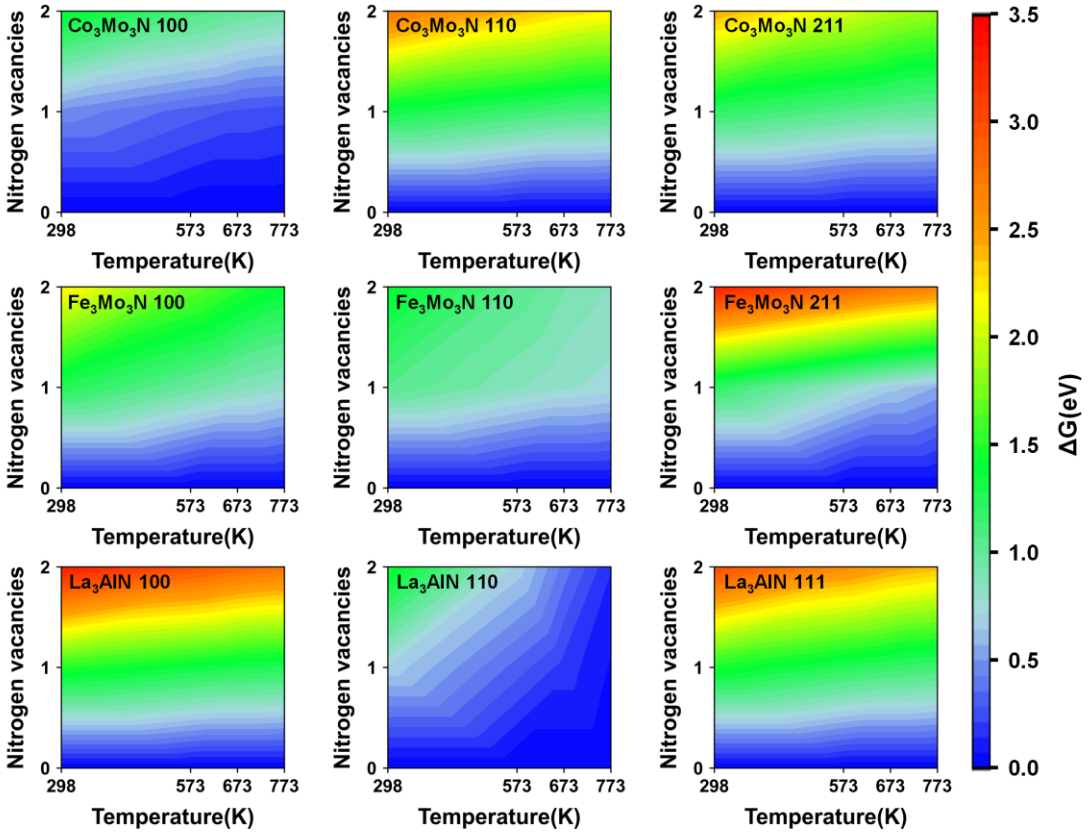

Fig. S3 Relative free energies of formation of N vacancies on the surface of Co_3Mo_3N, Fe_3Mo_3N and La_3AlN catalysts at 298, 573, 673, 773 K and 1 bar.

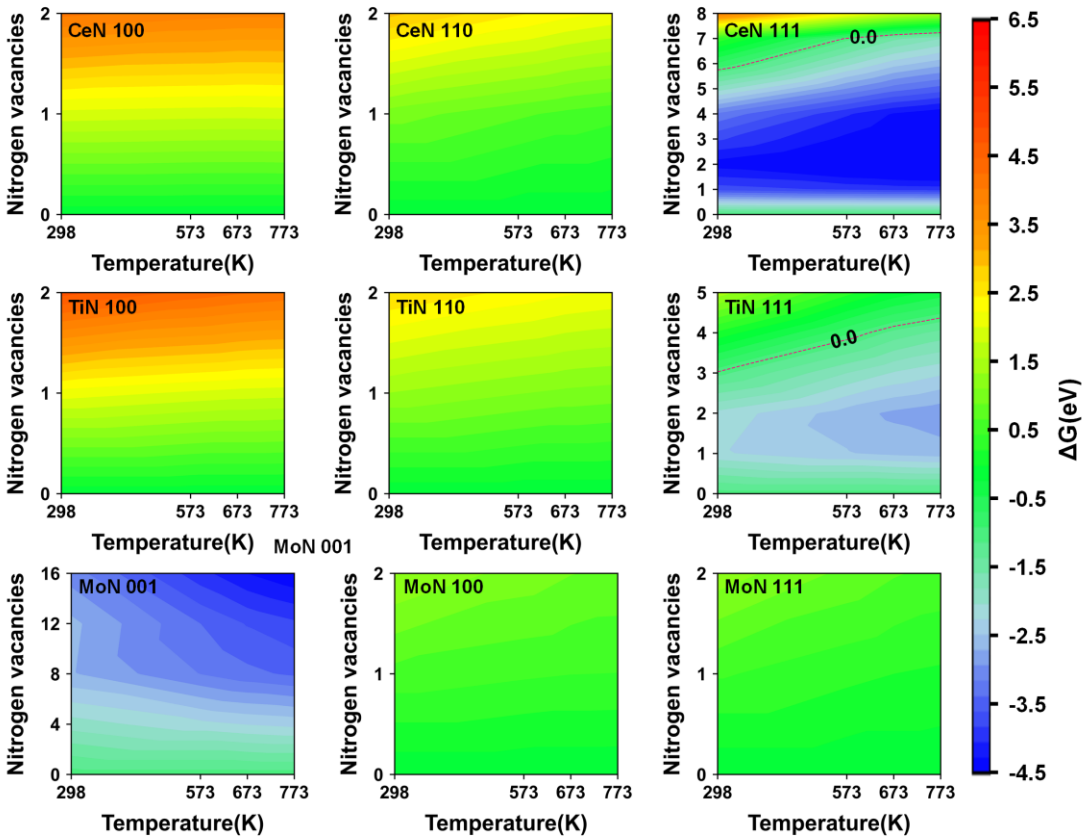

Fig. S4 Relative free energies of formation of N vacancies on the surface of CeN, TiN and MoN catalysts at 298, 573, 673, 773 K and 1 bar.

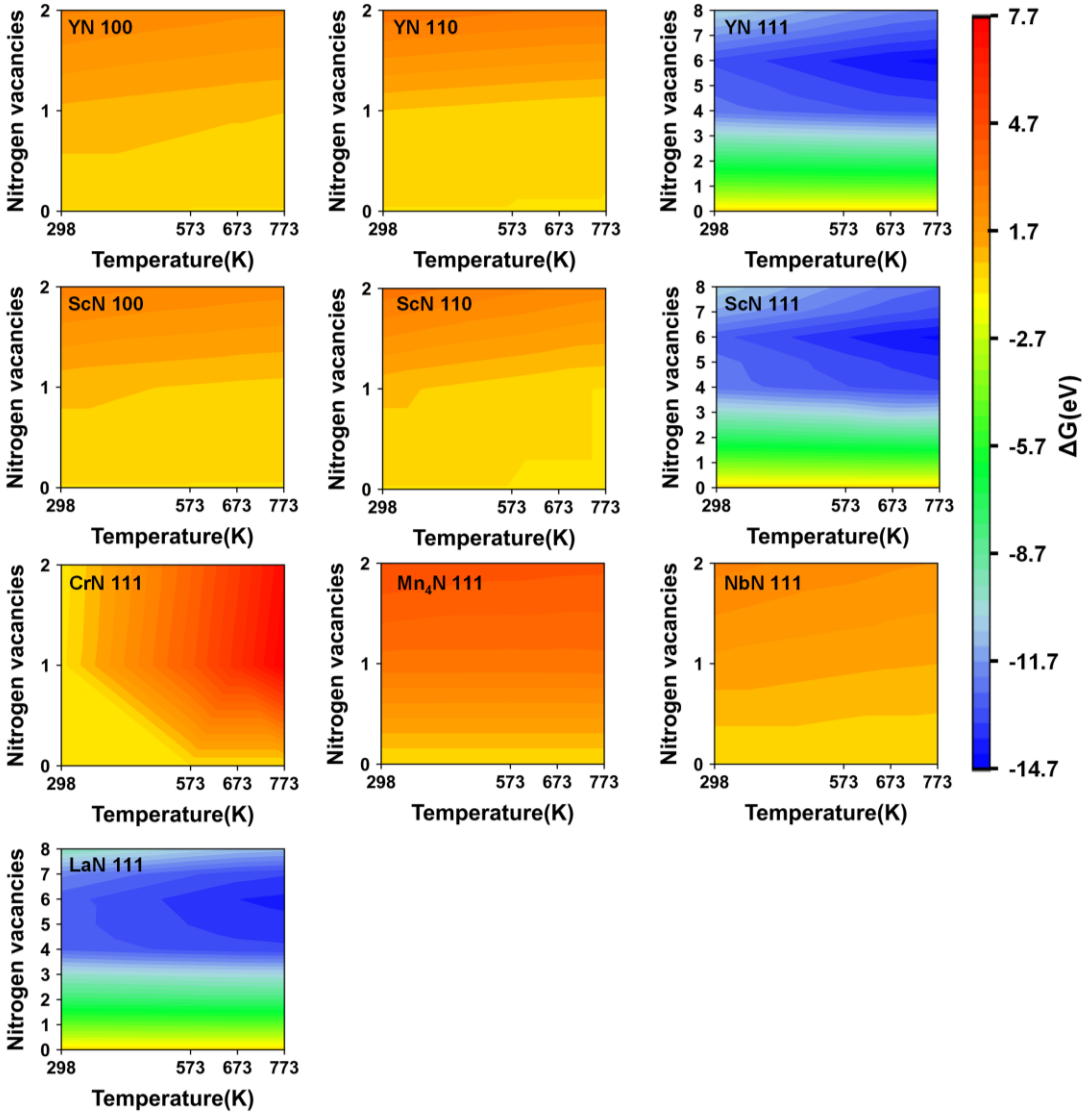

Fig. S5 Relative free energies of formation of N vacancies on the surface of YN, ScN, CrN, Mn_4N, NbN and LaN catalysts at 298, 573, 673, 773 K and 1 bar.

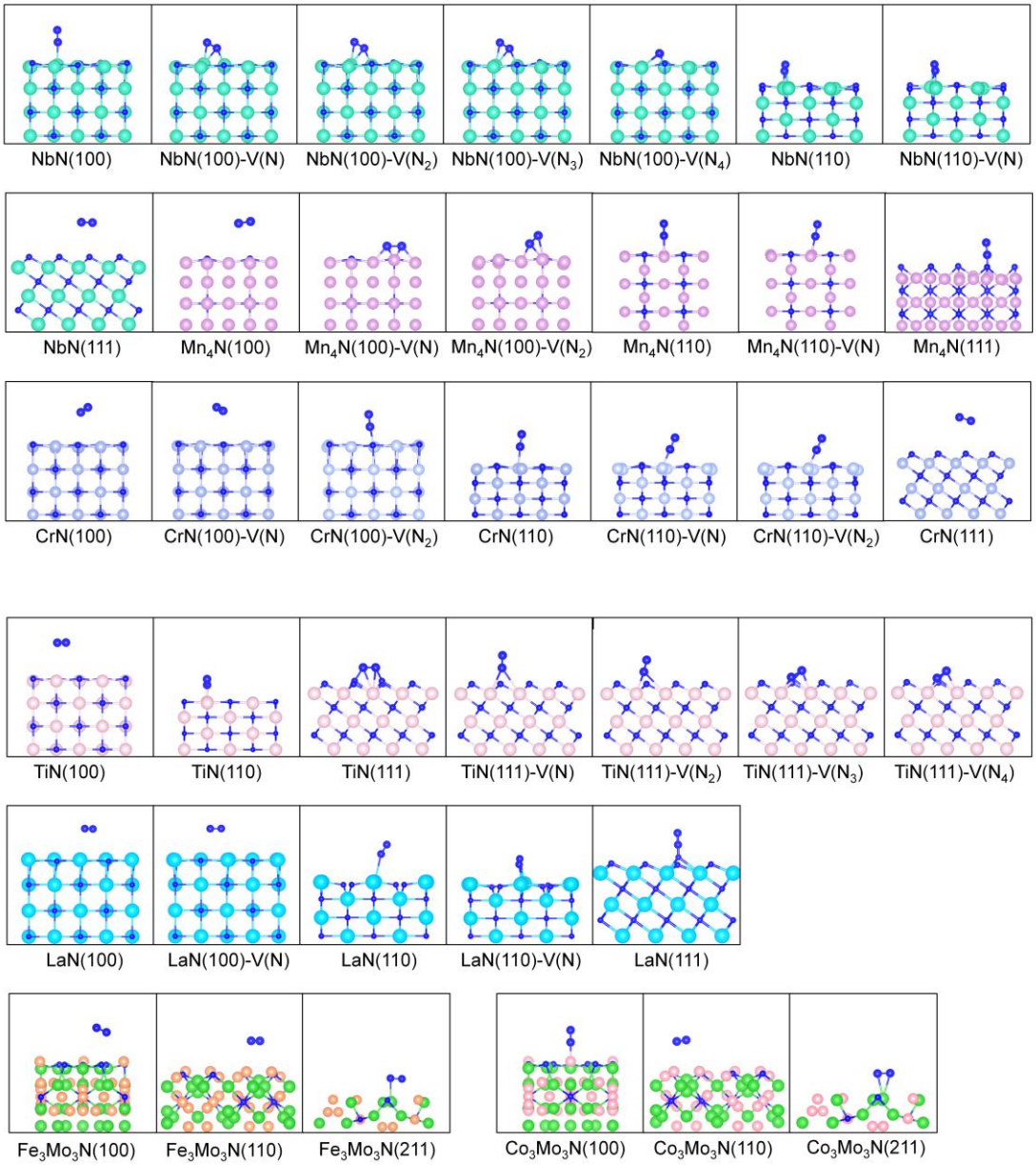

Fig. S6 Optimized configurations of N_2 adsorption.

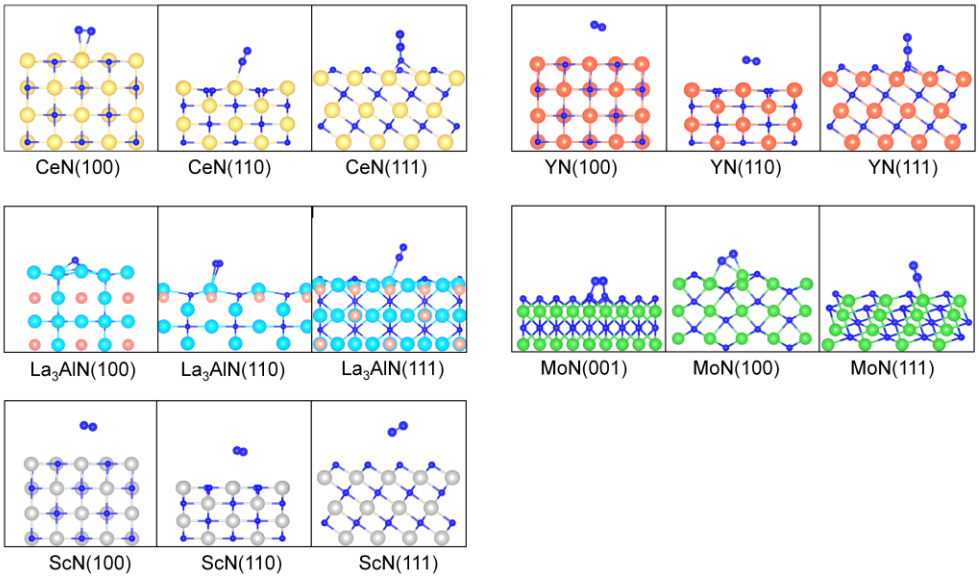

Fig. S7 Optimized configurations of N_2 adsorption.

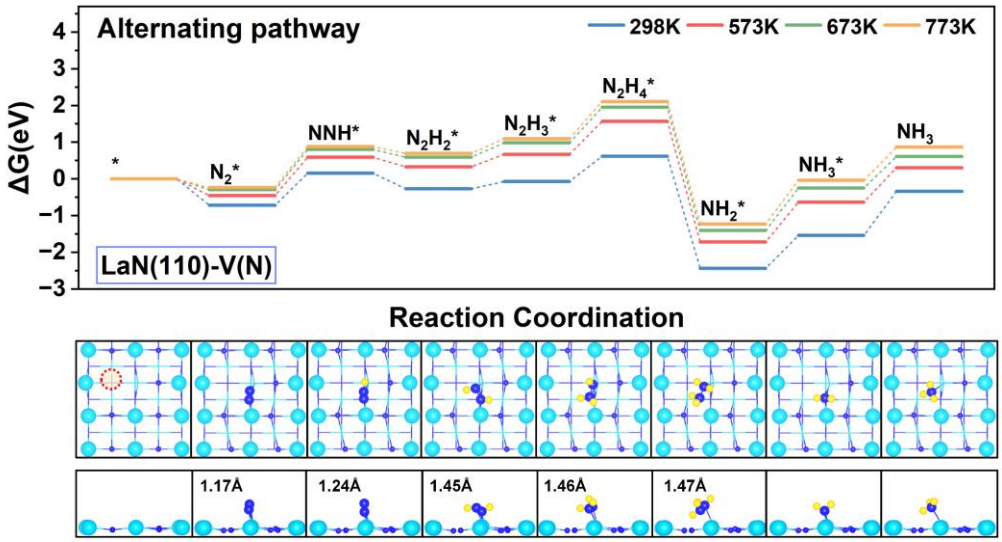

Fig. S8 Free energy diagrams of ammonia synthesis on LaN(110)-V(N) surface via an alternating reaction pathway. The free energies were calculated at 298K, 573 K, 673K, 773K and 1 bar (H_2/N_2 ratio is fixed at 3:1, which is consistent with the experimental conditions.

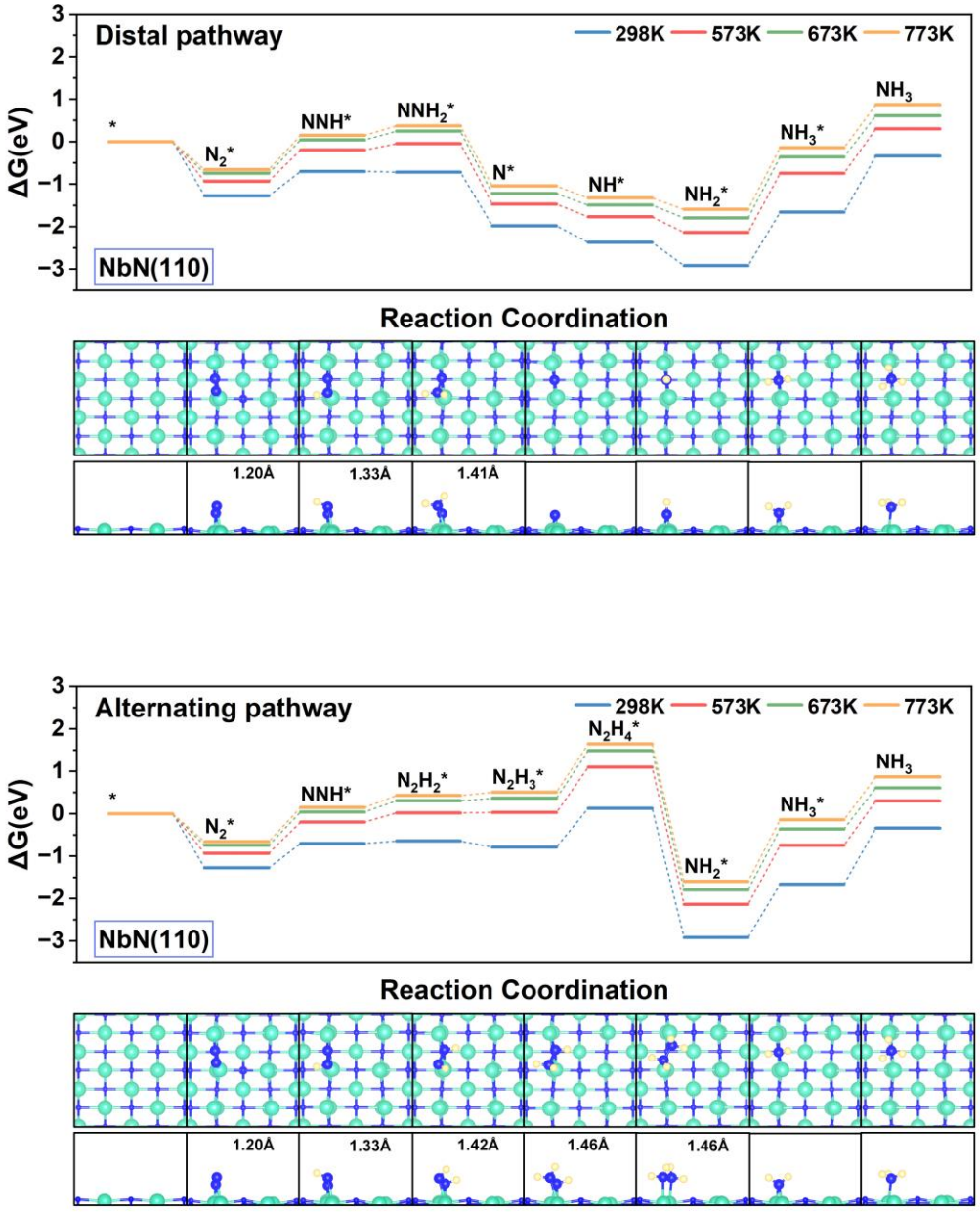

Fig. S9 Free energy diagrams of ammonia synthesis on NbN(110) surfaces via a distal reaction pathway and an alternating reaction pathway. The free energies were calculated at 573 K and 1 bar (H_2/N_2 ratio is fixed at 3:1, which is consistent with the experimental conditions.

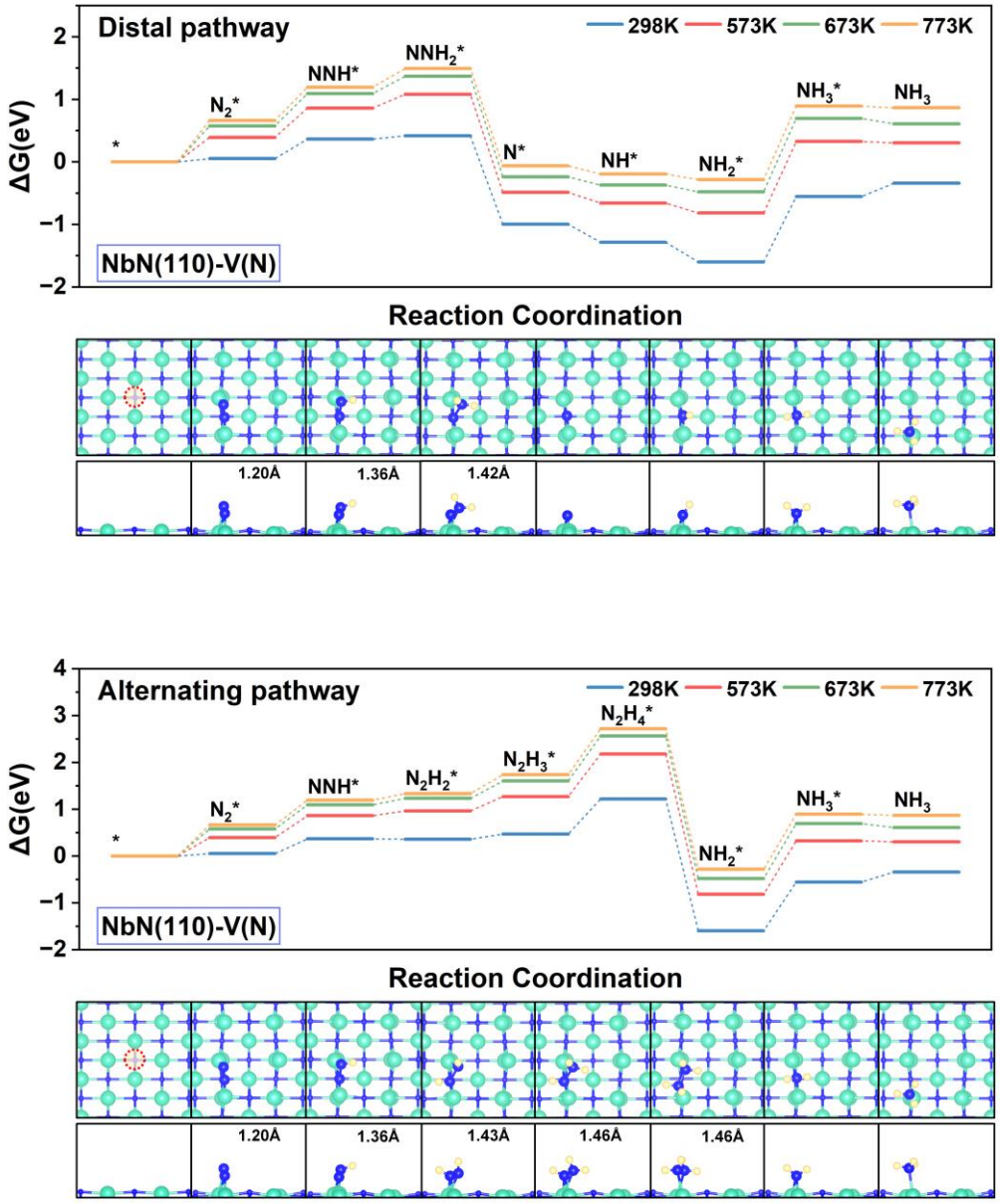

Fig. S10 Free energy diagrams of ammonia synthesis on NbN(110)-V(N) surfaces via a distal reaction pathway and an alternating reaction pathway. The free energies were calculated at 573 K and 1 bar (H_2/N_2 ratio is fixed at 3:1, which is consistent with the experimental conditions.

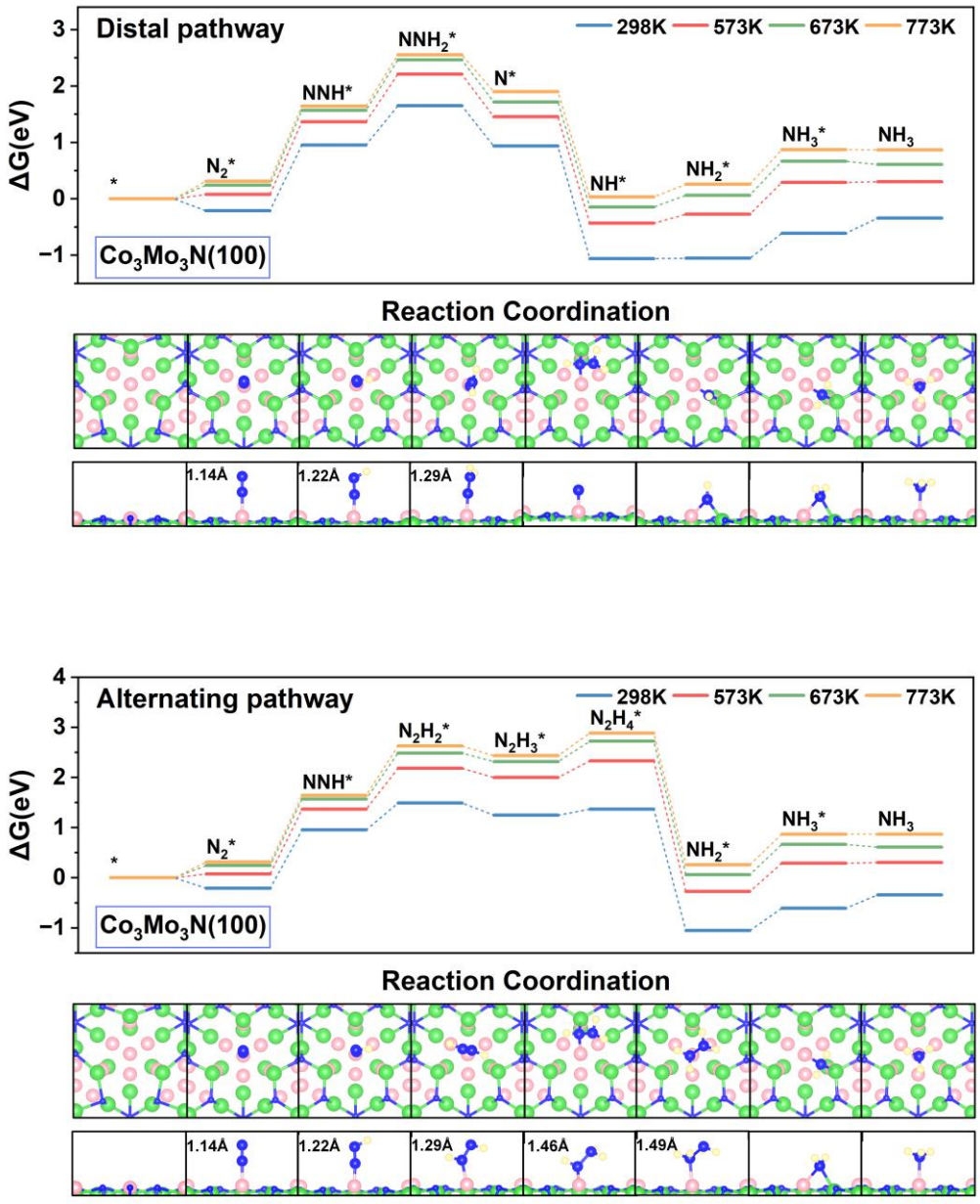

Fig. S11 Free energy diagrams of ammonia synthesis on $Co_3Mo_3N(100)$ surfaces via a distal reaction pathway and an alternating reaction pathway. The free energies were calculated at 573 K and 1 bar (H_2/N_2 ratio is fixed at 3:1, which is consistent with the experimental conditions.

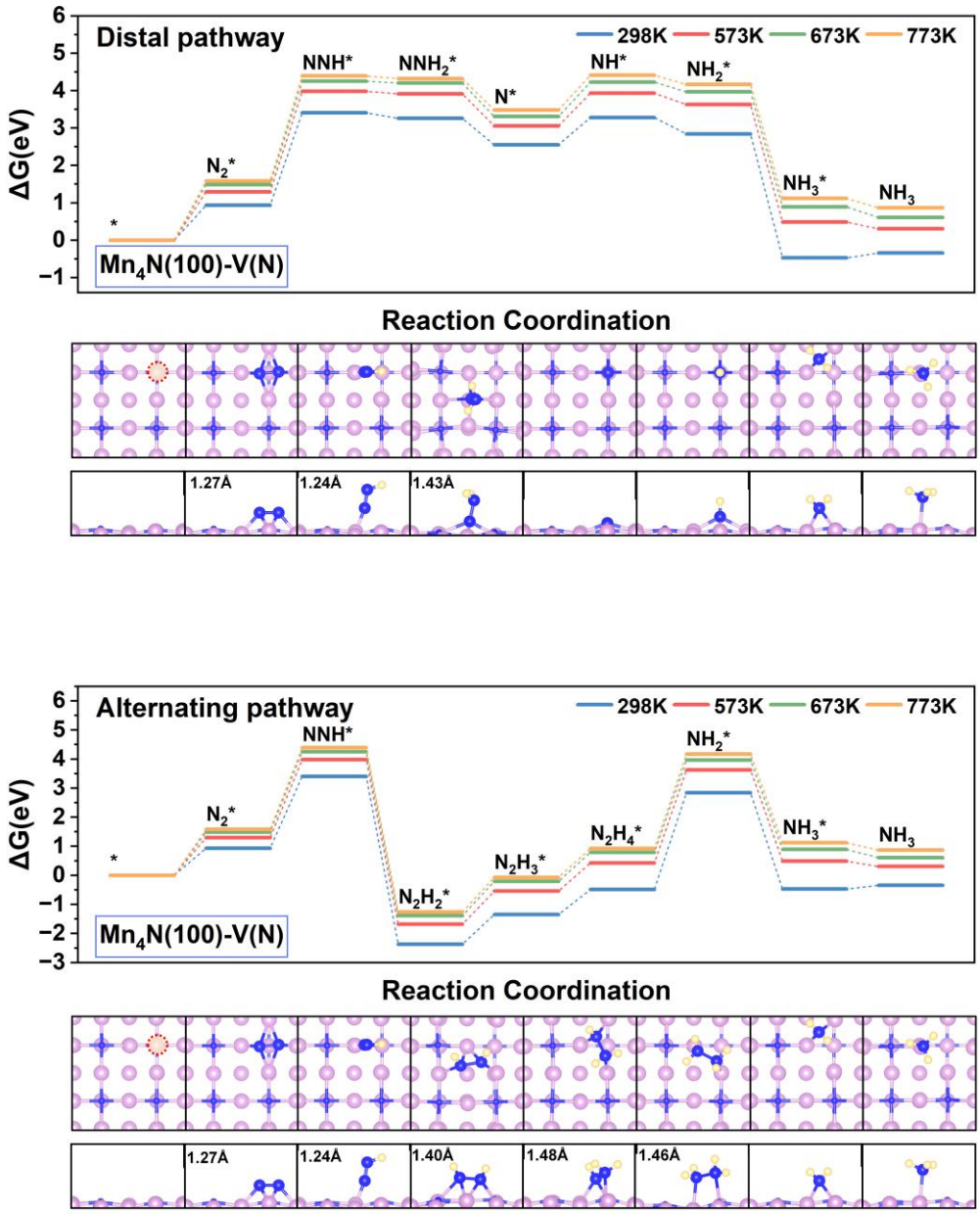

Fig. S12 Free energy diagrams of ammonia synthesis on $Mn_4N(100)$-V(N) surfaces via a distal reaction pathway and an alternating reaction pathway. The free energies were calculated at 573 K and 1 bar (H_2/N_2 ratio is fixed at 3:1, which is consistent with the experimental conditions.

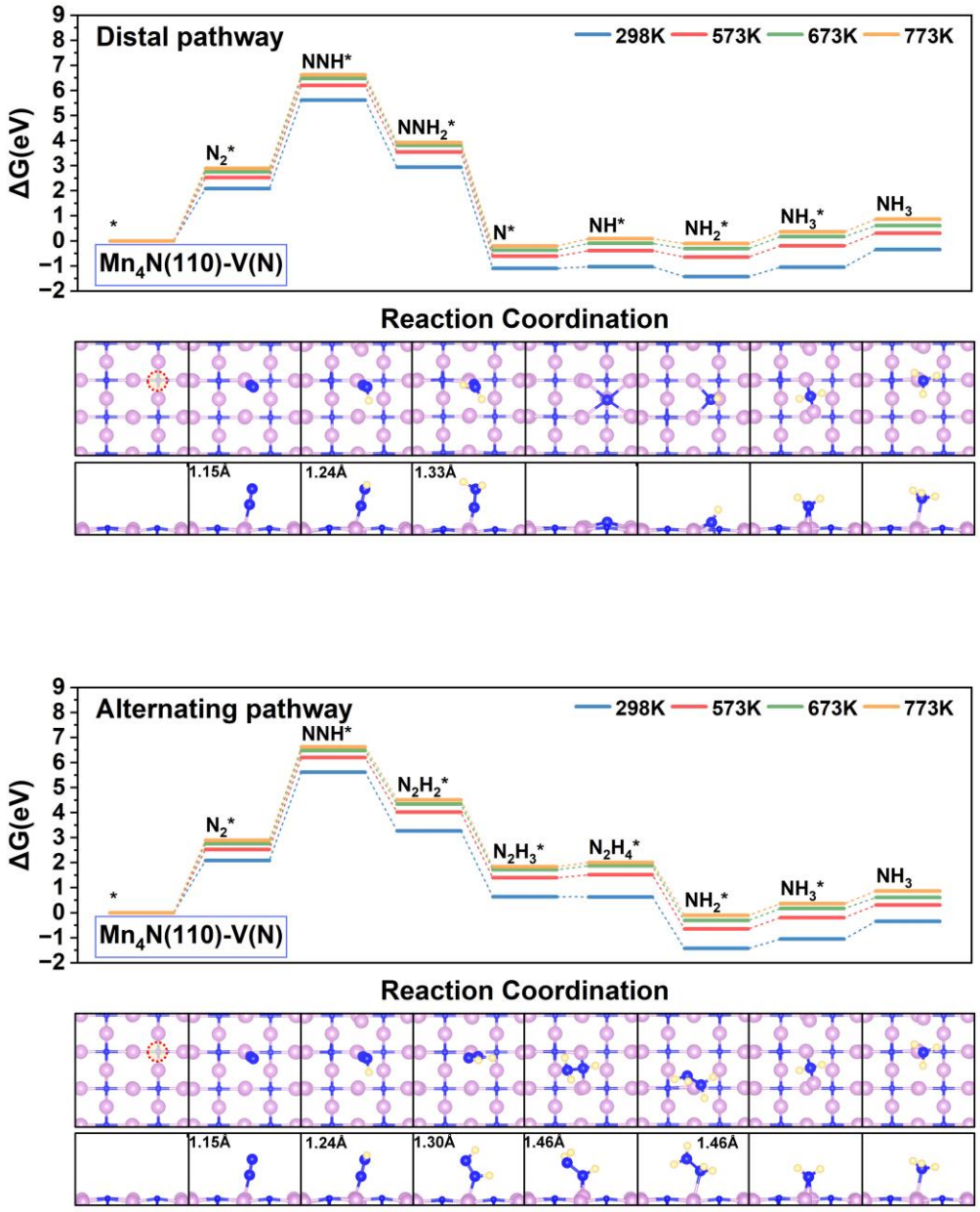

Fig. S13 Free energy diagrams of ammonia synthesis on $Mn_4N(110)$-V(N) surfaces via a distal reaction pathway and an alternating reaction pathway. The free energies were calculated at 573 K and 1 bar (H_2/N_2 ratio is fixed at 3:1, which is consistent with the experimental conditions.

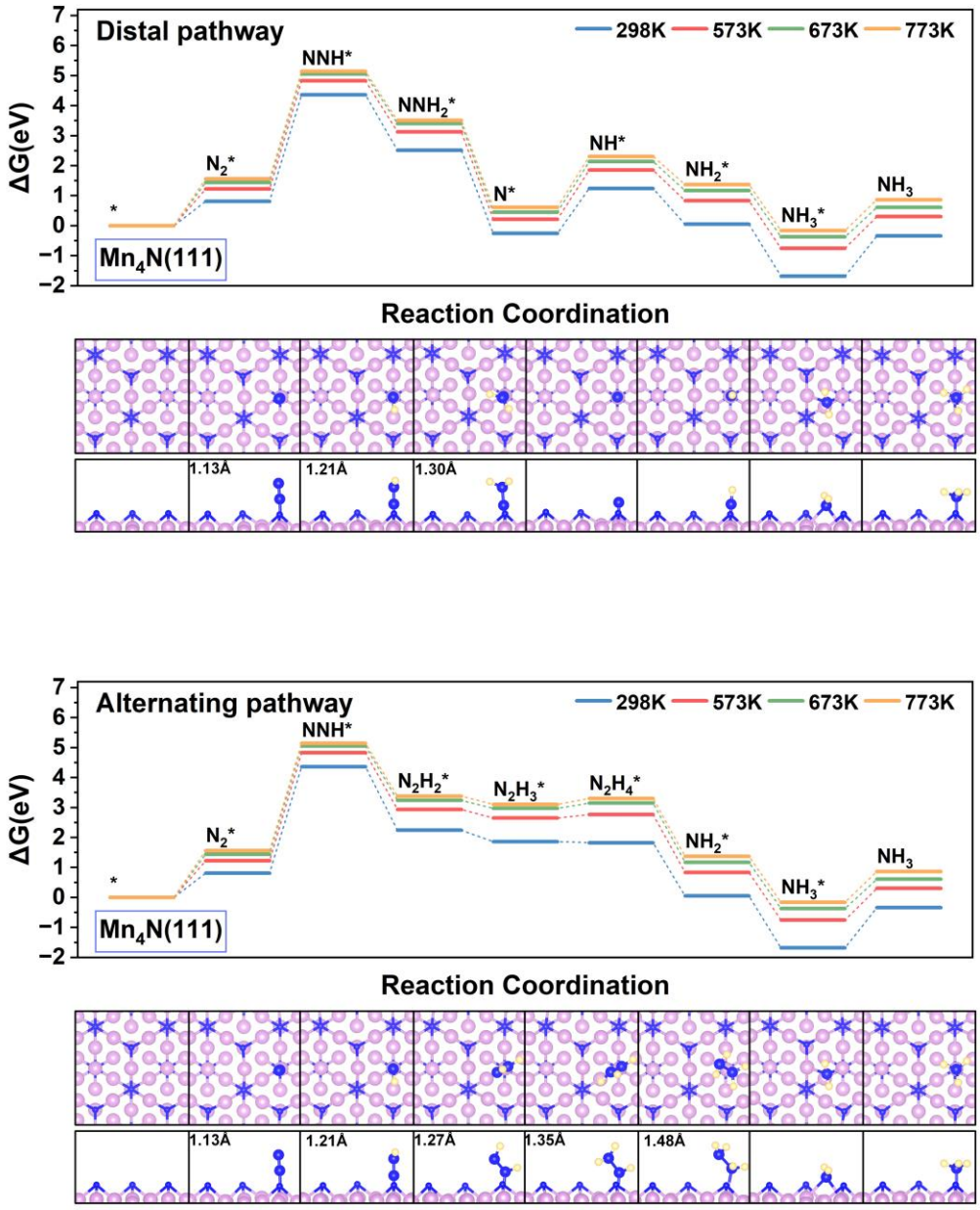

Fig. S14 Free energy diagrams of ammonia synthesis on $Mn_4N(111)$ surfaces via a distal reaction pathway and an alternating reaction pathway. The free energies were calculated at 573 K and 1 bar (H_2/N_2 ratio is fixed at 3:1, which is consistent with the experimental conditions.

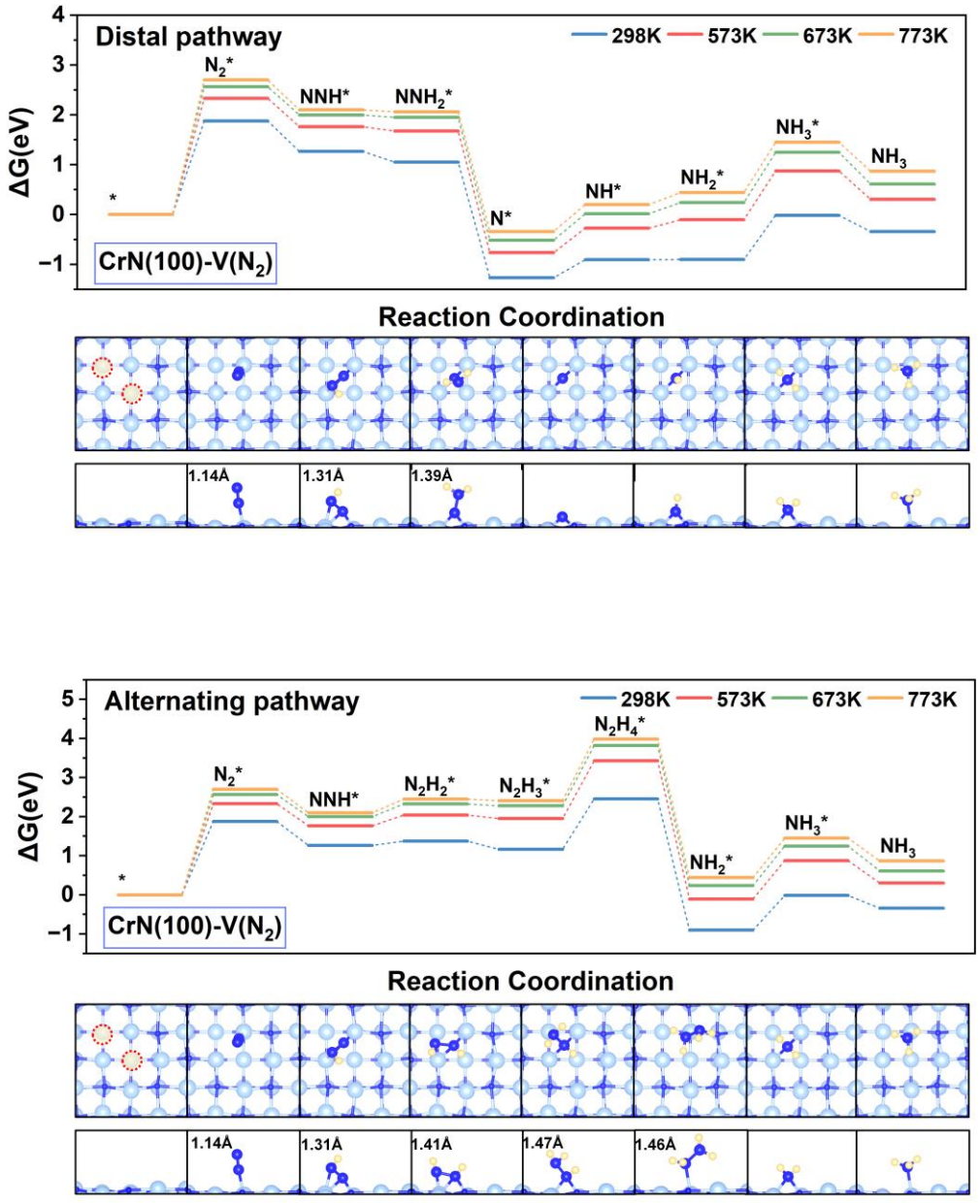

Fig. S15 Free energy diagrams of ammonia synthesis on CrN(100)-V(N_2) surfaces via a distal reaction pathway and an alternating reaction pathway. The free energies were calculated at 573 K and 1 bar (H_2/N_2 ratio is fixed at 3:1, which is consistent with the experimental conditions.

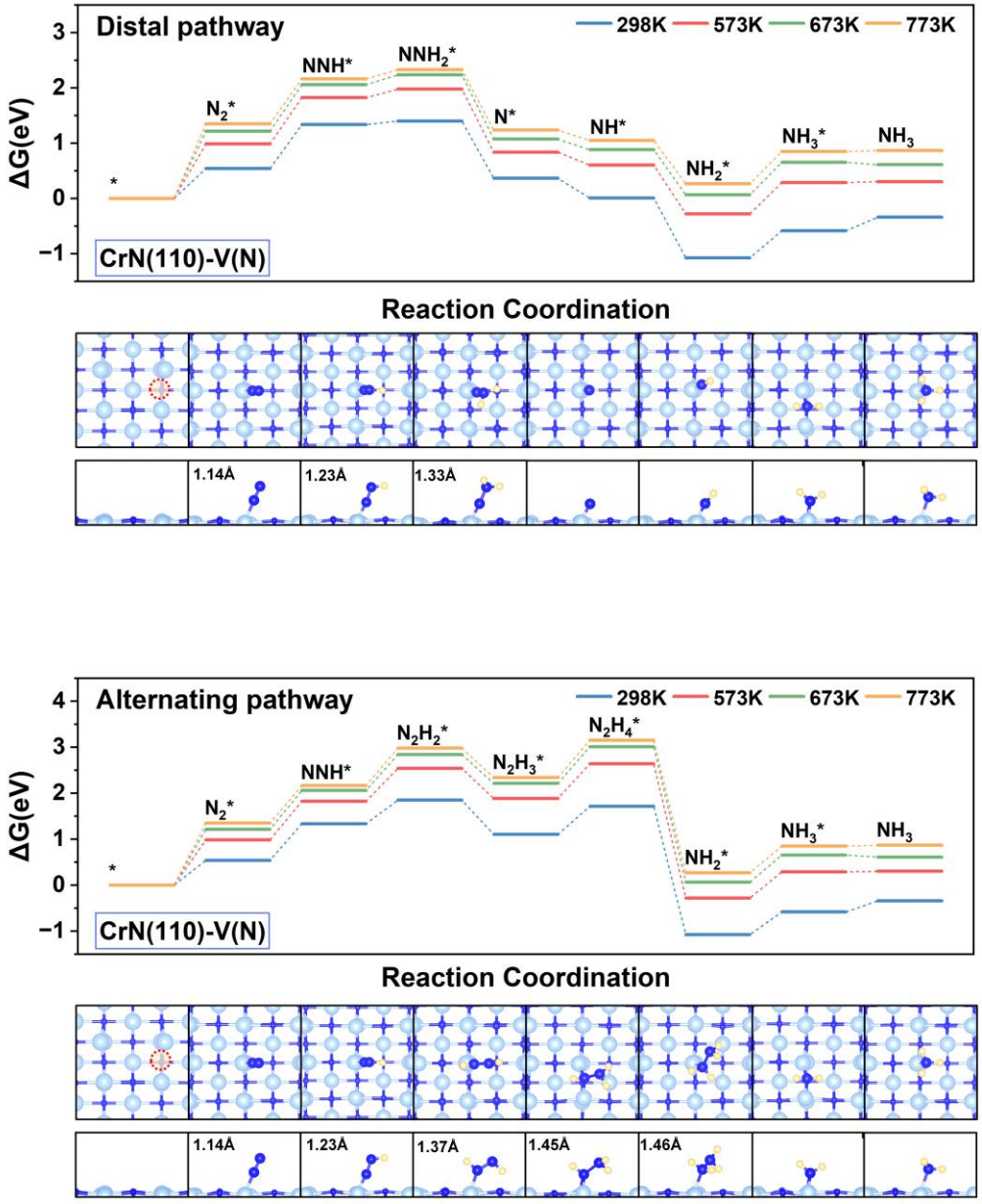

Fig. S16 Free energy diagrams of ammonia synthesis on CrN(110)-V(N) surfaces via a distal reaction pathway and an alternating reaction pathway. The free energies were calculated at 573 K and 1 bar (H_2/N_2 ratio is fixed at 3:1, which is consistent with the experimental conditions.

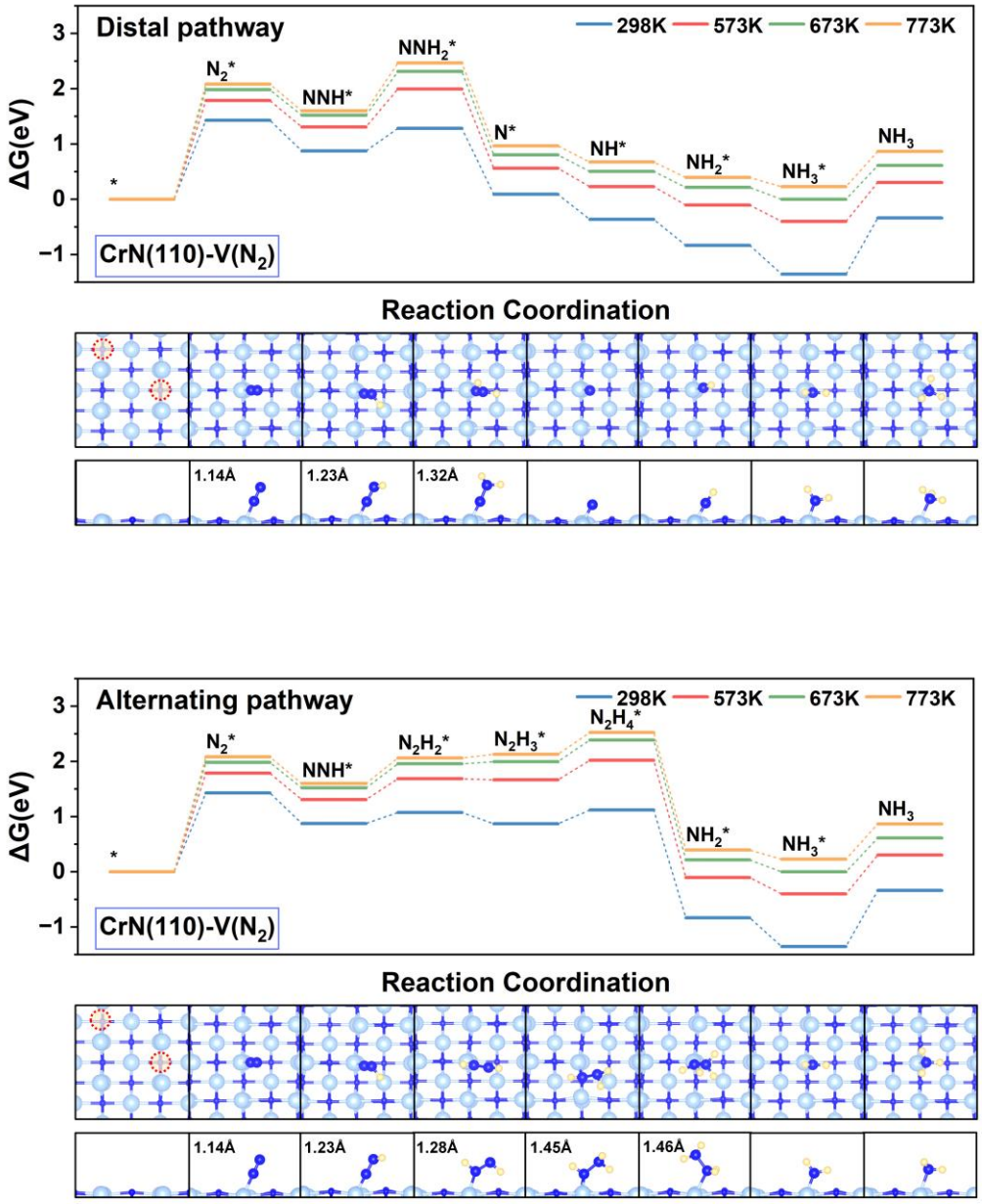

Fig. S17 Free energy diagrams of ammonia synthesis on CrN(110)-V(N_2) surfaces via a distal reaction pathway and an alternating reaction pathway. The free energies were calculated at 573 K and 1 bar (H_2/N_2 ratio is fixed at 3:1, which is consistent with the experimental conditions.

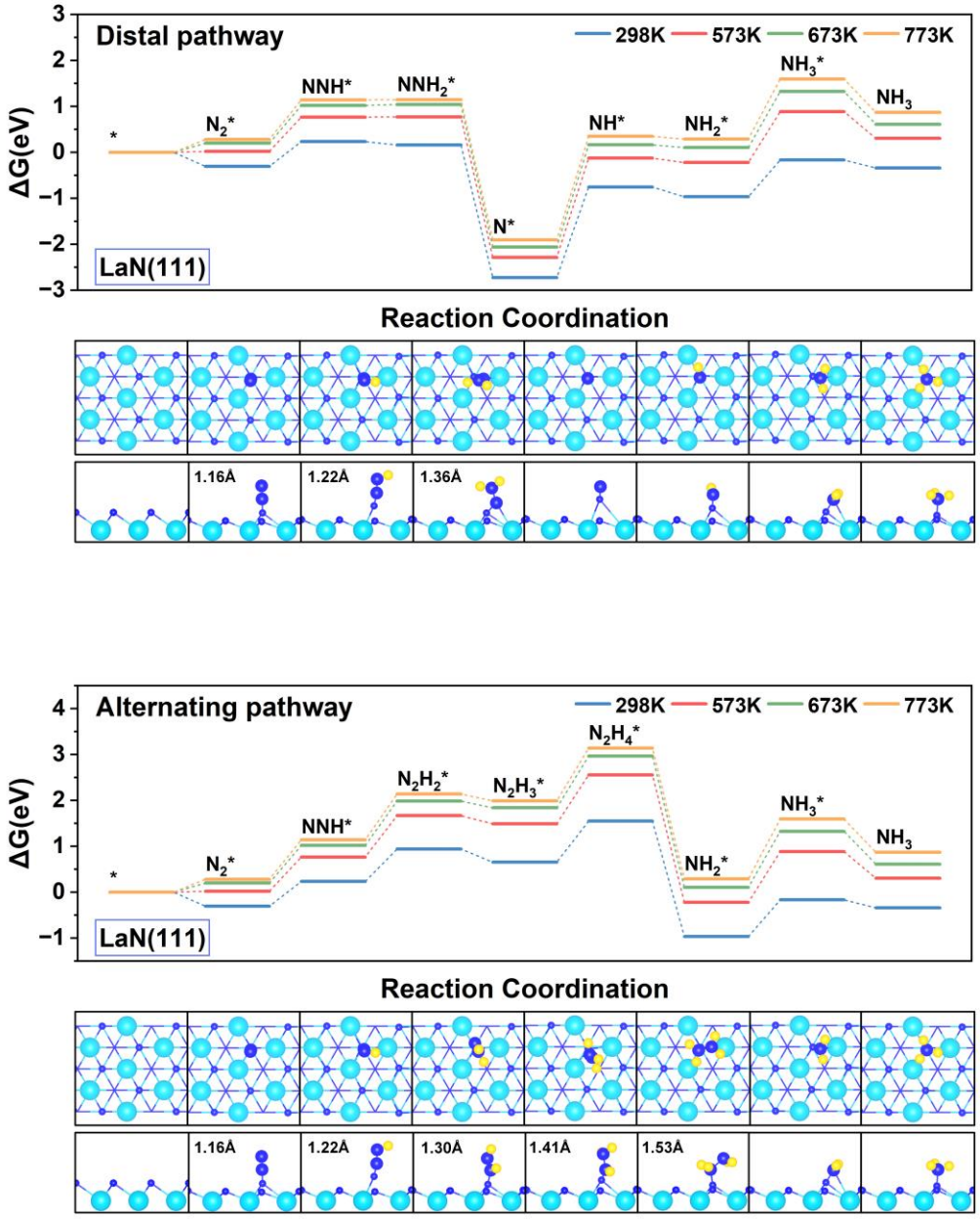

Fig. S18 Free energy diagrams of ammonia synthesis on LaN(111) surfaces via a distal reaction pathway and an alternating reaction pathway. The free energies were calculated at 573 K and 1 bar (H_2/N_2 ratio is fixed at 3:1, which is consistent with the experimental conditions.

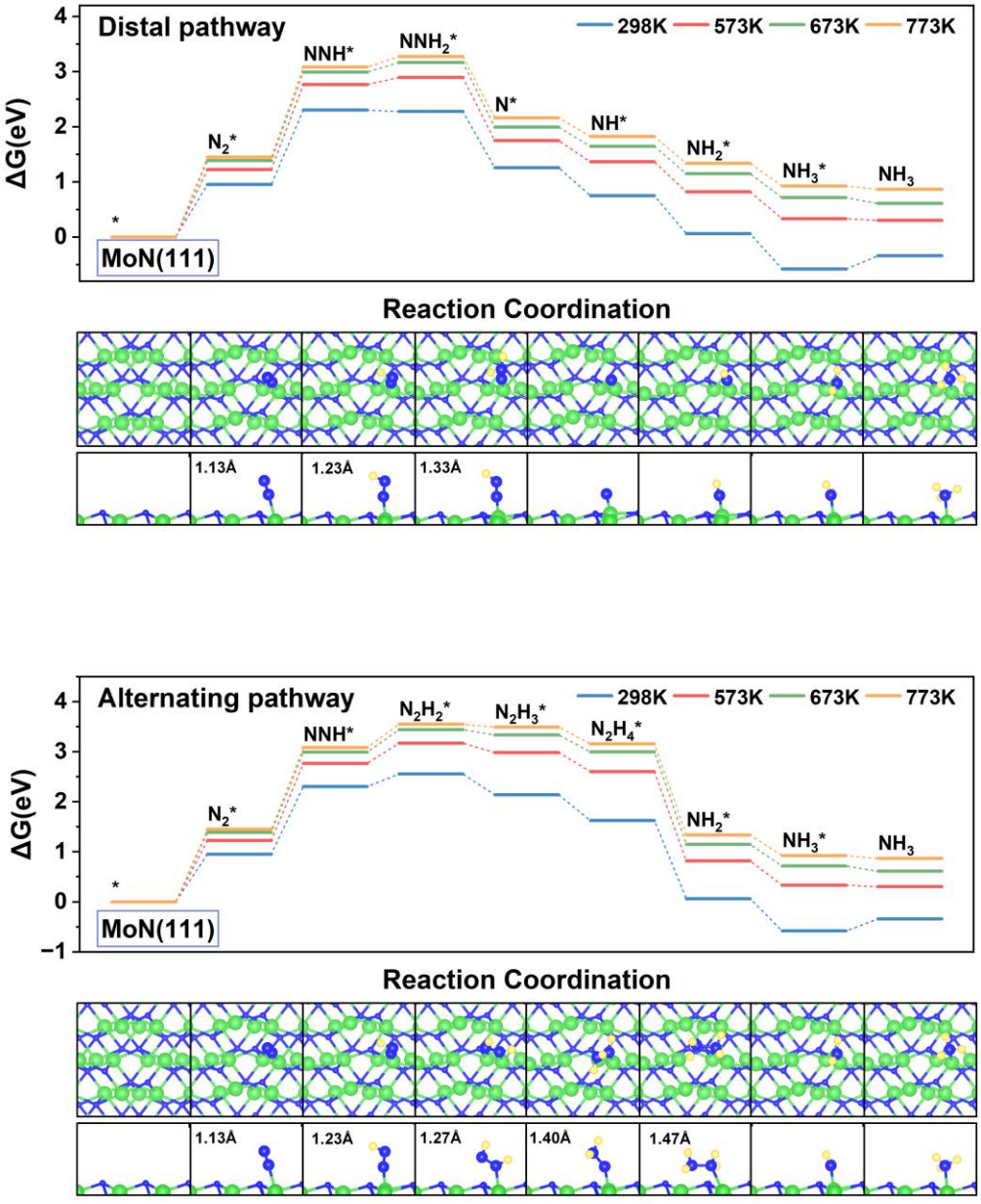

Fig. S19 Free energy diagrams of ammonia synthesis on MoN(111) surfaces via a distal reaction pathway and an alternating reaction pathway. The free energies were calculated at 573 K and 1 bar (H_2/N_2 ratio is fixed at 3:1, which is consistent with the experimental conditions.

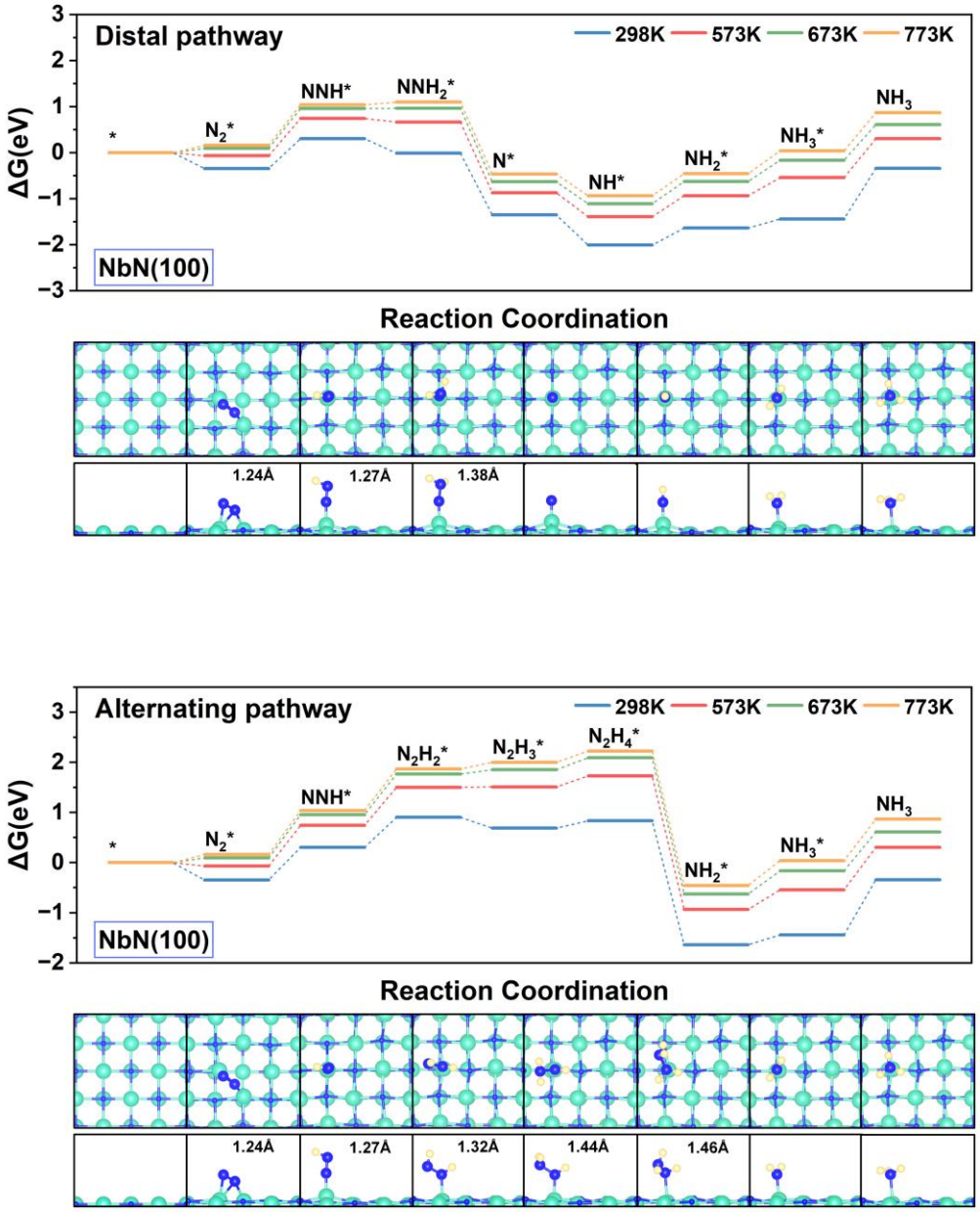

Fig. S20 Free energy diagrams of ammonia synthesis on NbN(100) surfaces via a distal reaction pathway and an alternating reaction pathway. The free energies were calculated at 573 K and 1 bar (H_2/N_2 ratio is fixed at 3:1, which is consistent with the experimental conditions.

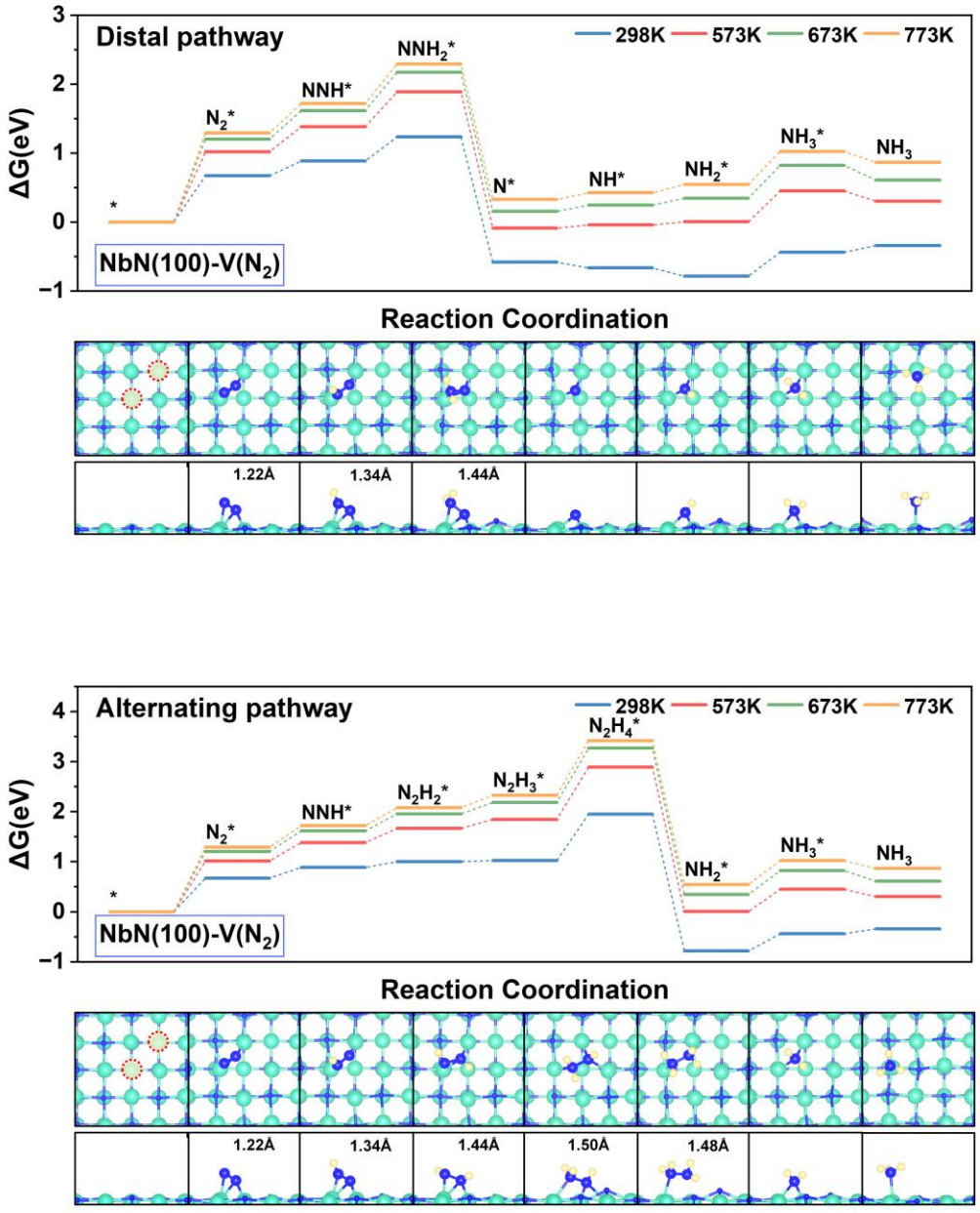

Fig. S21 Free energy diagrams of ammonia synthesis on NbN(100)-V(N_2) surfaces via a distal reaction pathway and an alternating reaction pathway. The free energies were calculated at 573 K and 1 bar (H_2/N_2 ratio is fixed at 3:1, which is consistent with the experimental conditions.

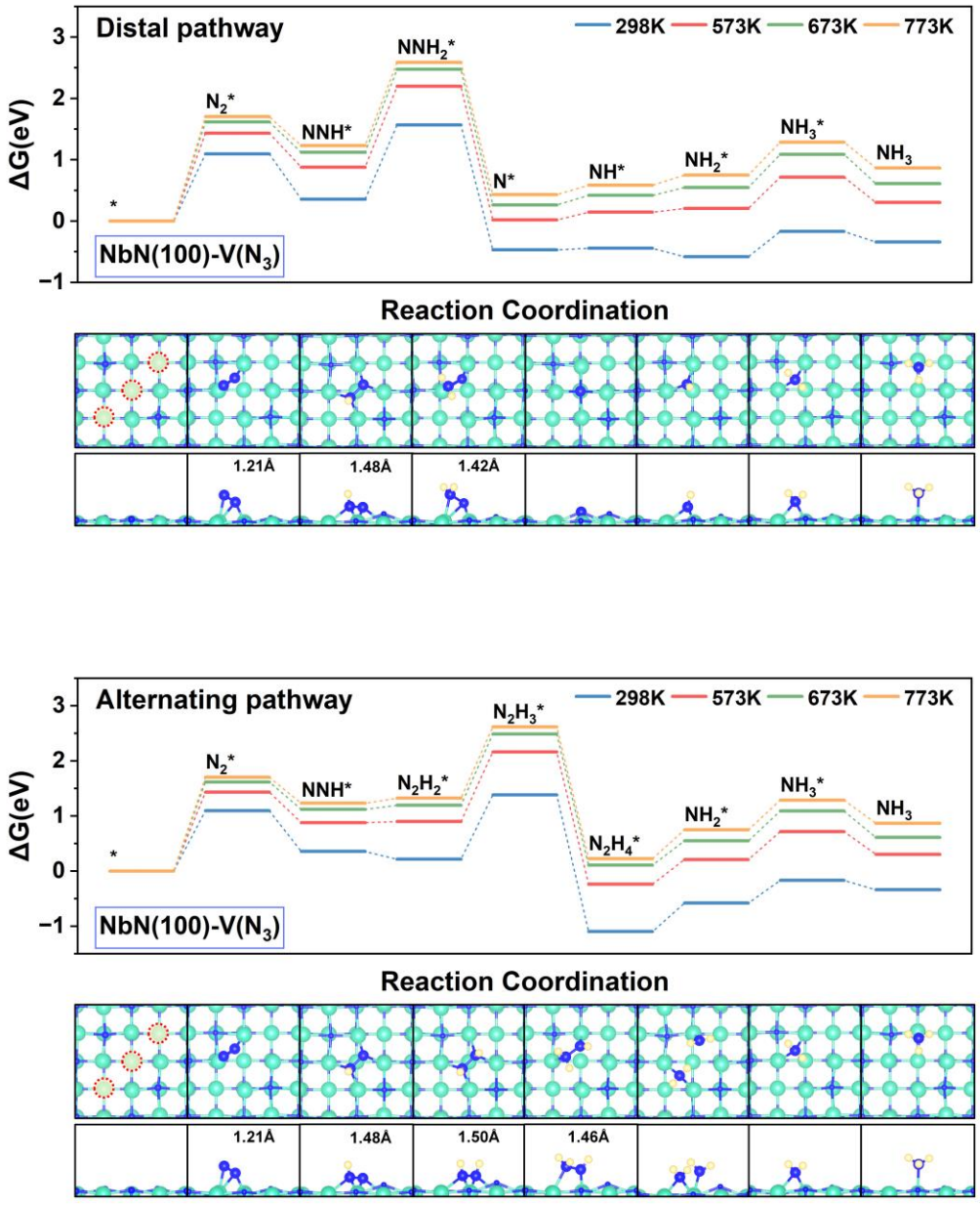

Fig. S22 Free energy diagrams of ammonia synthesis on NbN(100)-V(N_3) surfaces via a distal reaction pathway and an alternating reaction pathway. The free energies were calculated at 573 K and 1 bar (H_2/N_2 ratio is fixed at 3:1, which is consistent with the experimental conditions.

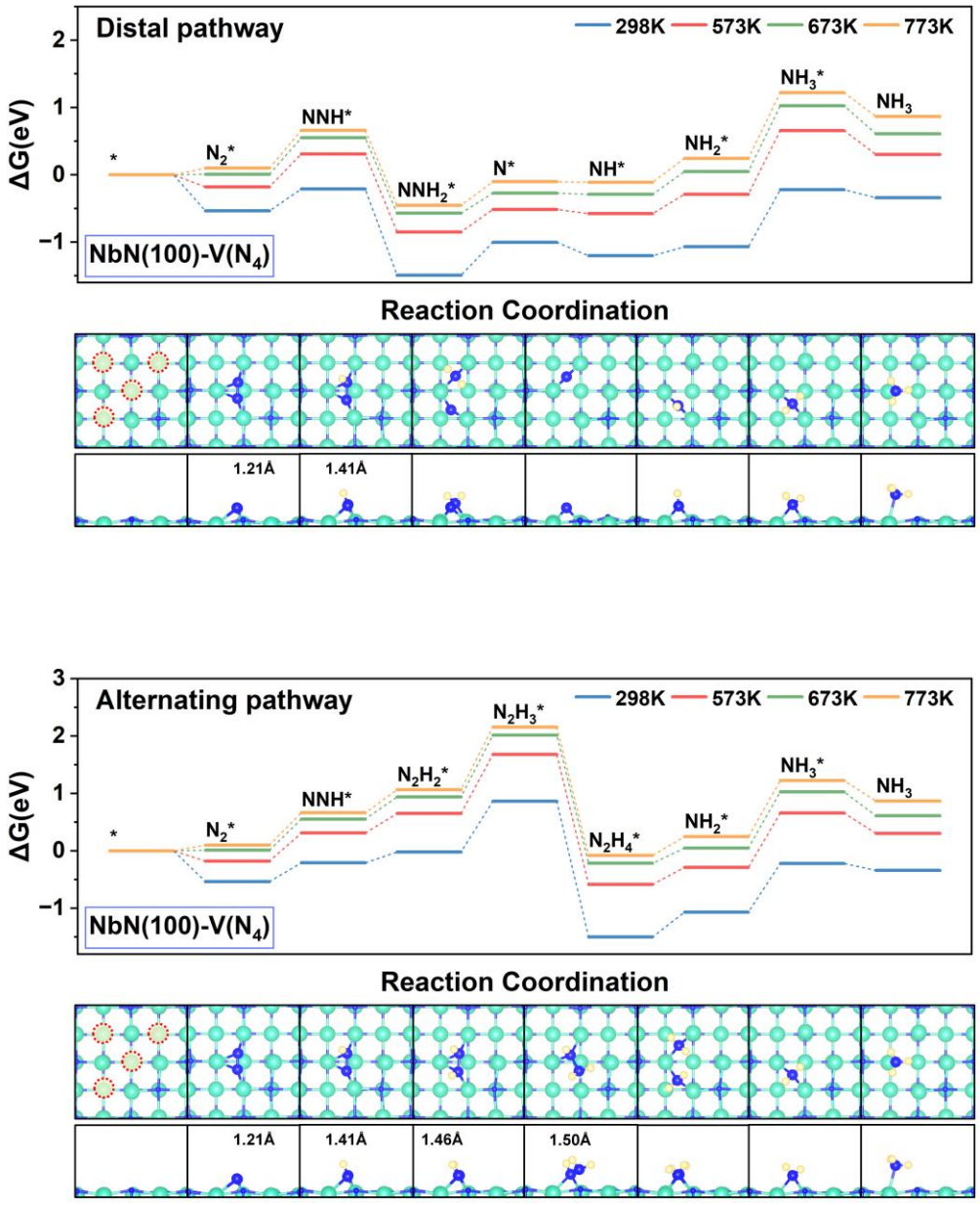

Fig. S23 Free energy diagrams of ammonia synthesis on NbN(100)-V(N_4) surfaces via a distal reaction pathway and an alternating reaction pathway. The free energies were calculated at 573 K and 1 bar (H_2/N_2 ratio is fixed at 3:1, which is consistent with the experimental conditions.

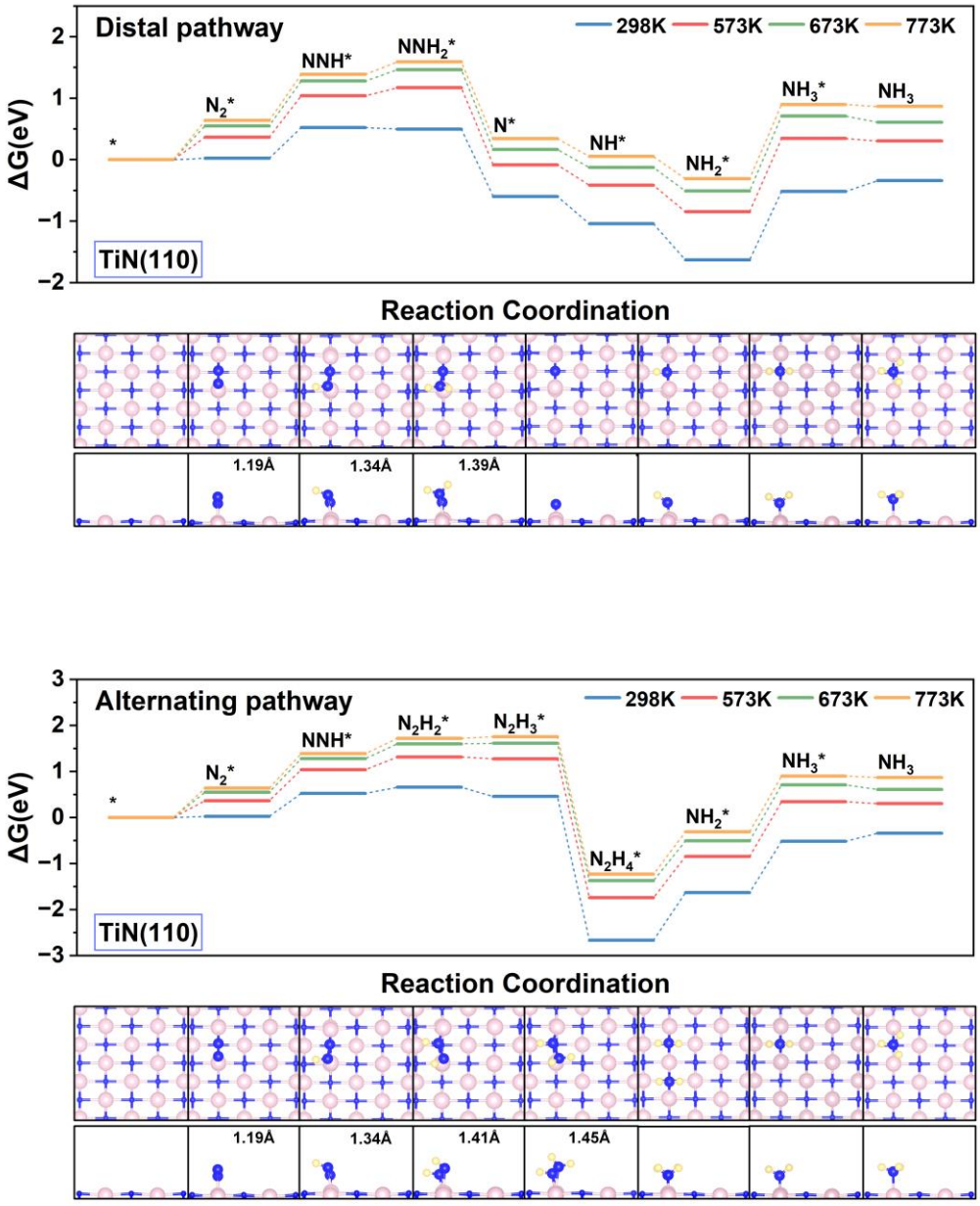

Fig. S24 Free energy diagrams of ammonia synthesis on TiN(110) surfaces via a distal reaction pathway and an alternating reaction pathway. The free energies were calculated at 573 K and 1 bar (H_2/N_2 ratio is fixed at 3:1, which is consistent with the experimental conditions.

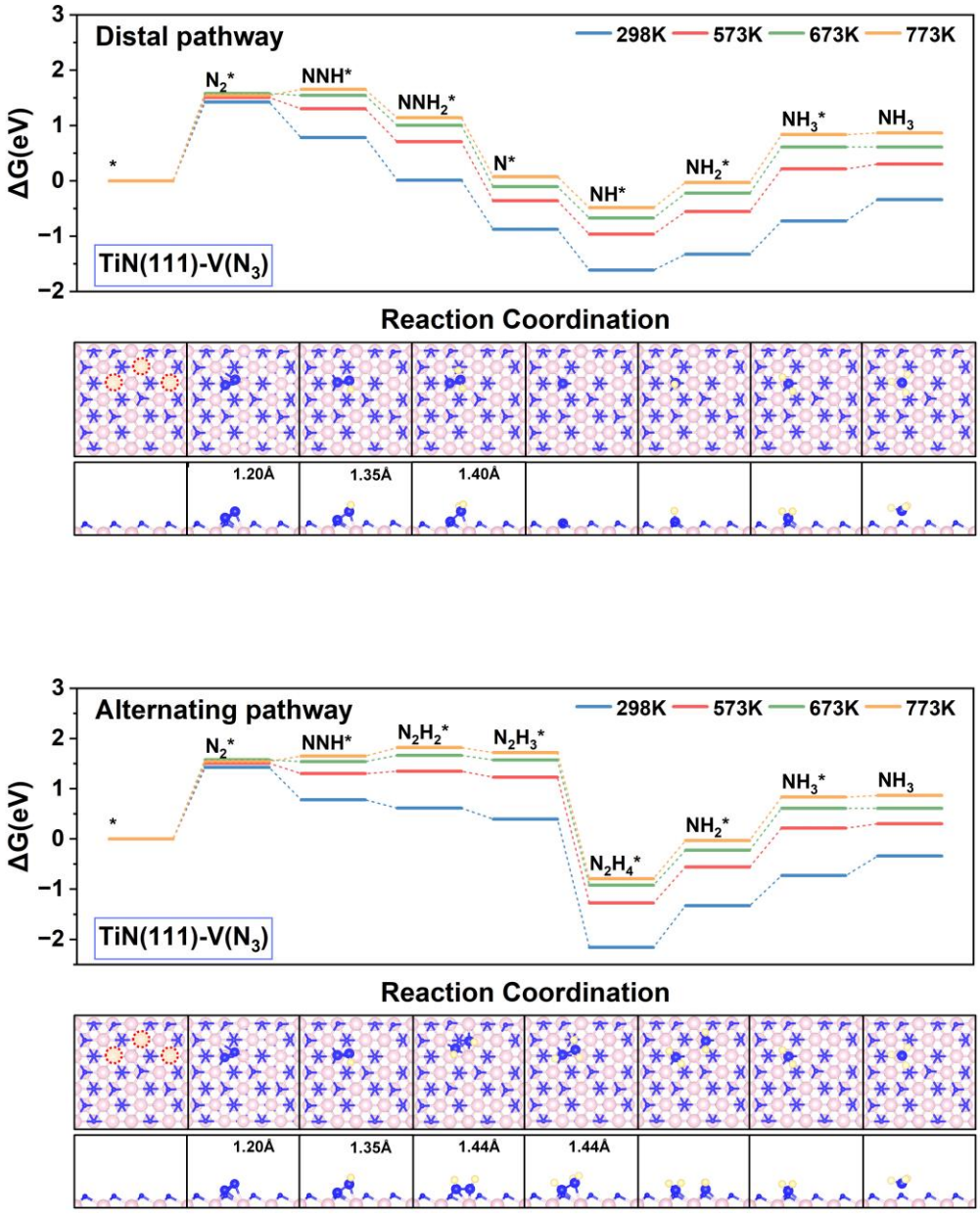

Fig. S25 Free energy diagrams of ammonia synthesis on TiN(111)-V(N_3) surfaces via a distal reaction pathway and an alternating reaction pathway. The free energies were calculated at 573 K and 1 bar (H_2/N_2 ratio is fixed at 3:1, which is consistent with the experimental conditions.

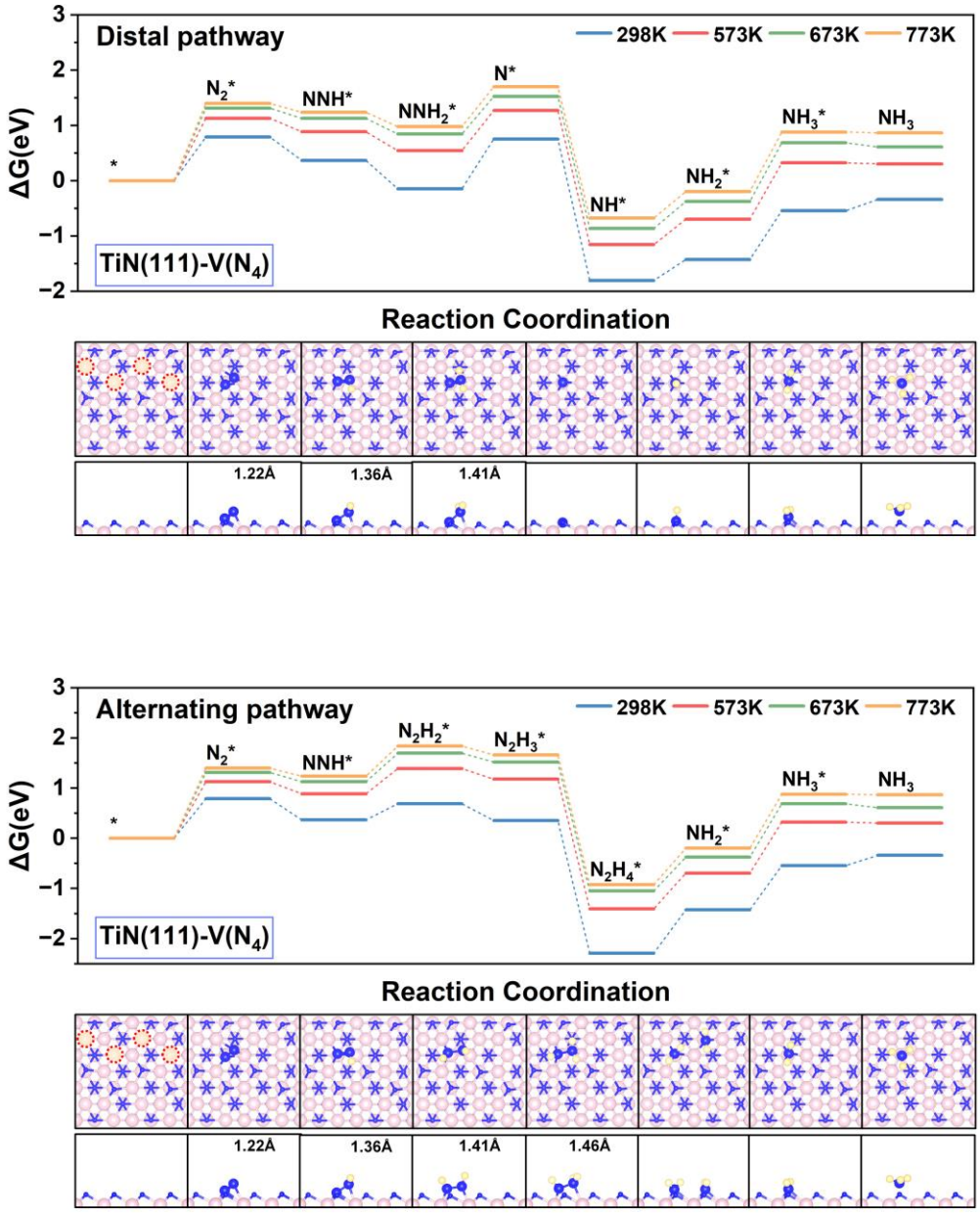

Fig. S26 Free energy diagrams of ammonia synthesis on TiN(111)-V(N_4) surfaces via a distal reaction pathway and an alternating reaction pathway. The free energies were calculated at 573 K and 1 bar (H_2/N_2 ratio is fixed at 3:1, which is consistent with the experimental conditions.

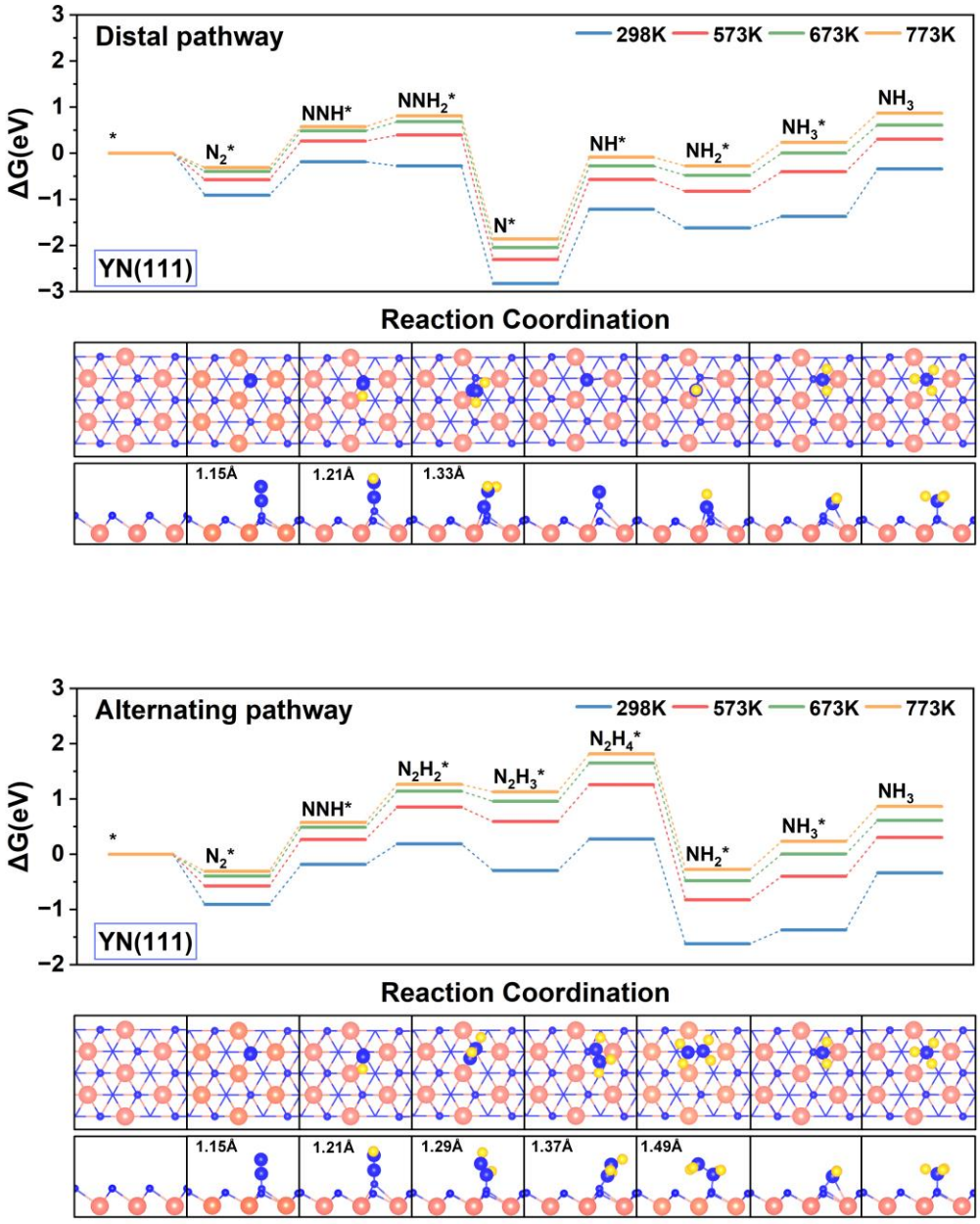

Fig. S27 Free energy diagrams of ammonia synthesis on YN(111) surfaces via a distal reaction pathway and an alternating reaction pathway. The free energies were calculated at 573 K and 1 bar (H_2/N_2 ratio is fixed at 3:1, which is consistent with the experimental conditions.